Spatial-temporal Variations and Process Analysis of O_3 Pollution in Hangzhou during the G20 Summit

By

Zhi-zhen Ni[1], Kun Luo[1*], Yang Gao[2], Xiang Gao[1], Fei Jiang[3], Cheng Huang[4], Jian-ren Fan[1], Joshua S. Fu[5], Chang-hong Chen[4]

[1]State Key Laboratory of Clean Energy, Department of Energy Engineering, Zhejiang University, Hangzhou 310027, China

[2] Key Laboratory of Marine Environment and Ecology, Ministry of Education of China, Ocean University of China, Qingdao 266100, China

[3]International Institute for Earth System Science, Nanjing University, Nanjing, China

[4]Shanghai Academy of Environmental Sciences, Shanghai 200233, China

[5]Civil & Environmental Engineering, the University of Tennessee, Neyland, UK

Submitted to

Atmospheric Chemistry and Physics

[*]Correspondence to: zjulk@zju.edu.cn

Abstract

Serious urban ozone (O_3) pollution was observed during the campaign of 2016 G20 summit in Hangzhou, China, while other pollutants had been significantly reduced by the short-term emission control measures. To understand the underlying mechanism, the Weather Research Forecast with Chemistry (WRF-Chem) model is used to investigate the spatial and temporal O_3 variations in Hangzhou from August 24 to September 6, 2016. The model is first successfully evaluated and validated for local and regional meteorological and chemical parameters by using the ground and upper-air level observed data. High ozone concentrations, temporarily during most day time of the emission control period and spatially from the surface to the top of the planetary boundary layer, are captured in Hangzhou and even the whole YRD region. Various atmospheric processes are further analyzed to determine the influential factors of local ozone formation through the integrated process rate method. Interesting horizontal and vertical advection circulations of O_3 are observed during several short periods, and the effects of these processes are nearly cancelled out. As a result, the ozone pollution is mainly attributed to the local photochemical reactions which are not obviously influenced by the emission reduction measures. The ratio of reduction of Volatile Organic Compounds (VOCs) to that of NO_x is a critical parameter that needs to be carefully considered for future alleviation of ozone formation. In addition, the vertical diffusion from the upper-air background O_3 also plays an important role in shaping the surface ozone concentration. These results provide insight into urban O_3 formation in Hangzhou and support the Model Intercomparison Study Asia Phase III (MICS-Asia Phase III).

Keywords: Ozone pollution, WRF-Chem, Spatial-temporal variation, Process analysis, Air quality.

1. Introduction

Tropospheric ozone (O_3) is generated by a series of photochemical reactions involving volatile organic compounds (VOCs), nitrogen oxide (NO_x), and carbon monoxide (CO) (Wang et al., 2006). As a primary component of photochemical smog, ground-level O_3 pollution imposes detrimental effects on human health (Ha et al., 2014; Kheirbek et al., 2013) and the ecosystem (Landry et al., 2013; Teixeira et al., 2011). However, O_3 pollution is a challenging problem worldwide. O_3 levels in cities in the United States and Europe are increasing more than those in the rural areas of these regions, where peak values gradually decreased during 1990–2010 (Paoletti et al., 2014). Nagashima et al., (2017) reported that long-term (1980–2005) trends of increase in surface O_3 over Japan may be primarily attributed to the continental transport that have contributed to photochemical O_3 production. Urban O_3 pollution events have also be observed in developing countries, such as Thailand (Zhang and Kim Oanh, 2002) and India (Calfapietra et al., 2016).

Many field monitoring and modeling studies have investigated the photochemical characteristics of near-surface O_3 pollution (Tang et al., 2009, 2012; Wang et al., 2013, 2014), the photochemistry of O_3 and its precursors (Xie et al., 2014), the interactions between O_3 and $PM_{2.5}$ (Shi et al., 2015), and the urban O_3 formation (Tie et al., 2013). It is clear that in addition to anthropogenic emissions of O_3 precursors, uncontrollable physical and chemical processes involved in meteorological phenomena significantly modulate changes in O_3 concentration (Xue et al., 2014). In the Yangtze River Delta (YRD) region of China, high O_3 concentrations have been observed (Gao et al., 2016; Jiang et al., 2012). Synoptic patterns related to tropical cyclones may be one reason for such high O_3 concentrations (Huang et al., 2005). Jiang et al. (2015) reported that enhanced stratosphere–troposphere exchange (STE) driven by a tropical cyclone abruptly increased O_3 concentrations (21–42 ppb) in the southeast of China during June 12–14, 2014, which has been highlighted as another contributor to near-surface O_3 concentrations under certain conditions (Lin et al., 2012, 2015). However, the complex dynamics in atmospheric processes related to O_3 formation

are so difficult to identify that the O_3 pollution characteristics and underlying causes have not yet been well understood.

Hangzhou, the capital of Zhejiang Province, is located in the center of the Yangtze River Delta which is one of the most developed areas in China. Resultant from local emissions (Wu et al. 2014, Hu et al. 2015) and transboundary transport of aerosol and trace gases transport (Liu et al. 2015; Ni et al. 2018; Zhang et al. 2018), air pollution in Hangzhou has become serious in the recent years. In 2016, Hangzhou city would host the 2016 G20 (Group of Twenty Finance Ministers and Central Bank Governors) summit during September 4-6. To improve air quality for this event, 14-day temporarily strict air pollution alleviation measures had been taken to reduce air pollutant emissions in Hangzhou and surrounding areas from August 24 to September 6, 2016. The emission control scheme includes a coal-fired power plant capacity 50% reduction since August 24, followed by an "odd-even" on-road vehicle restriction since August 28, and further emergent VOC reduction from industrial sectors since September 1 to 6 (Ji et al. 2018; Li et al. 2019; Wu et al. 2019). These short-term measures provide a valuable opportunity to investigate the response of air quality to the emission reduction, understand the formation mechanisms of air pollution, and explore effective policies for long-term air pollution control in the local or regional scale.

The effects of emission control on air pollutants during this G20 Summit have been investigated by several studies using field observations and numerical models. It is demonstrated that almost all major air pollutants including SO_2, NO_x (Li et al. 2019; Wu et al. 2019), fine particles (Ji et al. 2018; Li et al. 2019; Yu et al. 2018; Wu et al. 2019), and VOCs (Zheng et al. 2019) have been significantly reduced during the 14-day control period, except O3. Su et al. (2017) monitored the vertical profiles of ozone concentration in the lower troposphere of Hangzhou during the control period by using an ozone lidar. It was found that the ozone concentrations peaked near the top of the planetary boundary layer, and the temporary measures took no immediate effect on ozone pollution. Wu et al. (2019) investigated the variation of air pollution in Hangzhou and its surrounding areas during the G20 summit by using monitoring data from five sites, and reported

that the air quality had been greatly improved by the implementation of the emission control. However, the average O_3 concentration was increased by 19% compared to the same periods of the five preceding years. This unique response of ozone pollution to control measures is not well understood, and of great research interest for better control of ozone pollution in the future.

To this end, a regional air quality model, within the framework of the Model Inter-Comparison Study for ASIA phase III (Li et al., 2019), is used to investigate the spatial-temporal characteristics of ozone pollution in Hangzhou during the G20 Summit in the present work. Process analysis is conducted to understand the chemical and physical factors that contribute to O_3 abundance. It is found that the serious ozone pollution happened, mainly resultant from the local photochemical reactions which are not under good control by the emission reduction measures. The rest of this paper is organized as follows. Section 2 outlines the methodology and configuration of the model system. Section 3 presents the model evaluation, the spatial-temporal characteristics of ozone pollution, and the analysis of related atmospheric processes. Section 4 discusses the underlying causes of O_3 pollution. Finally, a summary is made.

2. Methodology

2.1. Regional chemistry modeling system

To investigate the interactions among emissions, meteorological phenomena, and chemical phenomena, the Weather Research Forecast with Chemistry model (WRF-Chem) is used in the present study. The WRF-Chem is a regional online-coupled air quality model that can simultaneously simulate air quality components and meteorological components by using identical transport schemes, grid structures, and physical schemes (Grell et al., 2005). Two model domains are designed: an outer domain (horizontal resolution: 30 km) covering East China (20.0°N–44.5°N, 99.0°E–126.5°E) and an inner domain (horizontal resolution: 6 km) covering the YRD region (27.6°N–32.7°N, 116.9°E–122.4°E), as shown in Fig.1. The “Lambert conformal conic” projection is applied with the domain center at 34°N, 111°E. A total of 31 vertical layers are used with the model top at 50 hPa. The simulation period is from 17 August to 6 September 2016, and the first-

week simulation is used to spin up the model. Hourly model outputs for 24 August to 06 September are used in the analysis. The gas mechanism CBMZ (Chemical Bond Mechanism Version Z) (Zaveri and Peters, 1999) is used for model simulations. For additional details regarding the model parameterization schemes, please refer to a previous study (Ni et al., 2018).

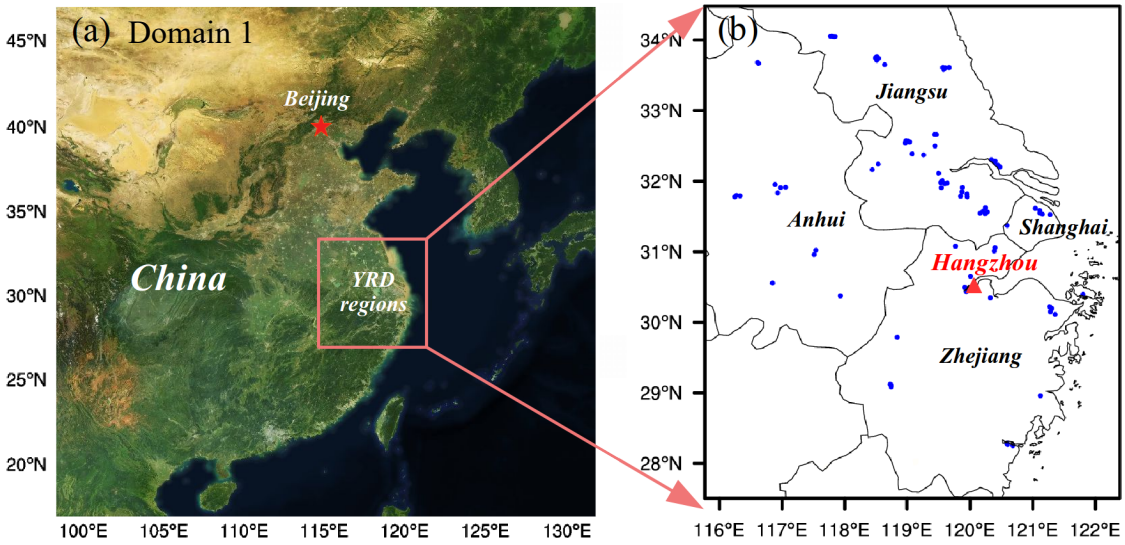

Fig. 1. Double-nested simulation domains. (a) Domain 1: 30 km in East China with 102 (W–E) × 111 (S–N) × 31 (vertical layers) grids; (b) Domain 2: 6 km in the Yangtze River Delta (YRD) region with 100 (W–E) × 115 (S–N) × 31 (vertical layers) grids. Blue dots denote the air quality monitoring sites. The copyright of the background map belongs to Google Map © Google.

The meteorological boundary and initial conditions are determined from the global objective final analysis (FNL) data of the National Centers for Environmental Prediction (Kalnay et al., 1996). The FNL data are mapped to domain 1 (East China), and the grid-nudging method (Stauffer et al., 1991) is used to reduce the meteorological integral errors. The chemical initial and boundary conditions are dynamically downscaled from the simulation results of model for ozone and related chemical tracers, version 4 (MOZART4) (Emmons et al., 2010).

2.2. Emissions

The 2016 Multiresolution Emission Inventory for China (MEIC, 0.25° × 0.25°; http://www.meicmodel.org/) is used for the outer domain (Fig. 1a) with a spatial resolution of 30 km (Li et al., 2017), including species of SO_2, NO_x, CO, NH_3, $PM_{2.5}$, and VOCs from the power,

industrial, residential, transportation, and agricultural sectors. Inventories of finer anthropogenic emissions for the YRD region over the year of 2014 compiled by Shanghai Academy of Environmental Sciences are used for the inner domain (Fig. 1b). These inventories have been well documented in previous studies (Huang et al., 2011; Li et al., 2011; Liu et al., 2018). The fine emission inventories include major sectors such as large point sources, industrial sources, mobile sources, and residential sources. The anthropogenic emissions over the YRD region are mainly located over the industrial and urban areas along the Yangtze River as well as over Hangzhou Bay. In this study, the emission inventories for the two domains are projected into horizontal and vertical grids as hourly emissions, with temporal and vertical profiles obtained from Wang et al. (2011). VOCs emissions are categorized into modeled species, according to von Schneidemesser et al. (2016). In addition, biogenic emissions are generated offline using the Model of Emission of Gases and Aerosols from Nature (MEGAN) (Guenther et al., 2006). Dust emissions are calculated online from surface features and meteorological fields by using the Air Force Weather Agency and Atmospheric and Environmental Research scheme (Jones et al., 2011). Other emissions, such as those from biomass burning, aviation, and sailing ships, accounting for very small fraction during this period, are therefore not considered here. However, it is worth noting that these base inventories have been modified in the simulation to reflect the realistic emissions according to the control measures taken in the period presented in the introduction.

2.3. Atmospheric processes analysis

To understand the underlying mechanism of O_3 formation, individual physical and chemical processes of O_3 formation are investigated by using the integrated process rate (IPR) analysis in the WRF-Chem model (Jfffries and Tonnesen, 1994). The IPR analysis differentiates changes in pollutant concentrations from individual atmospheric process which quantitatively elucidates the contributions of each process, mainly including advection, diffusion, emission, deposition, clouds process, aerosol and gaseous chemistry. The IPR analysis has been widely applied and demonstrated to be an effective tool for investigating the relative importance of individual processes and

interpreting O_3 concentrations (Goncalves et al., 2009; Tang et al., 2017; Shu et al., 2016). In the present work, we consider gas chemistry, vertical diffusion, horizontal and vertical advections as the main atmospheric processes for O_3 formation. Other processes, such as cloud process and horizontal diffusion, play minor roles and are thus not considered.

2.4. Evaluation metrics

To increase the confidence in interpretations of model results, model outputs should first be evaluated based on observations. Accordingly, the model results derived from domain 2 are compared with hourly surface observational data obtained from 96 air quality monitoring sites in the YRD region (blue dots, Fig. 1b) in this study. These observational data are downloaded from http://www.pm25.in, and O_3 as well as its precursor NO_2 are evaluated, in terms of statistical measures, namely the mean fractional bias (MFB), the mean fractional error (MFE), and the correlation coefficient (R), following the recommendation of the US Environmental Protection Agency (US EPA, 2007). Additionally, the meteorological parameters are evaluated based on the observational data, including temperature at 2 m (T2), relative humidity at 2 m (RH2), 10 m wind speed (WS10) and direction (WD10), from the Meteorological Assimilation Data Ingest System

Table 1. Discrete statistical indicators used in the model evaluation

Metrics	Definition	Range
Mean Fractional Bias (MFB)	$MFB = \frac{2}{N}\sum_{i=1}^{N}\frac{S_i - O_i}{S_i + O_i} \times 100\%$	-200% to 200%
Mean Fractional Error (MFE)	$MFE = \frac{2}{N}\sum_{i=1}^{N}\frac{\lvert S_i - O_i\rvert}{S_i + O_i} \times 100\%$	0 to 200%
Correlation Coefficient (r)	$r = \frac{\sum_{i=1}^{N}(S_i - \bar{S})(O_i - \bar{O})}{\sqrt{\sum_{i=1}^{N}(S_i - \bar{S})^2 \sum_{i=1}^{N}(O_i - \bar{O})^2}}$	0 to 1
Mean Bias (MB)	$MB = \frac{1}{N}\sum_{i=1}^{N}(S_i - O_i)$	-∞ to +∞
Gross Error (GE)	$GE = \frac{1}{N}\sum_{i=1}^{N}\lvert S_i - O_i\rvert$	0 to +∞
Root Mean Square Error (RMSE)	$RMSE = \sqrt{\frac{1}{N}\sum_{i=1}^{N}(S_i - O_i)^2}$	0 to +∞

N is the number of samples. S_i and O_i are values of simulations and observations at time or location i, respectively.

(https://madis.noaa.gov). Following the study of Zhang et al. (2014), commonly used mean bias (MB), gross error (GE), and root mean square error (RMSE) are calculated as the statistical indicators. All used statistical indicators are summarized in Table 1.

Besides the above evaluation of single-point based time series results, the vertical spatial distribution of modeled O_3 in Hangzhou is also evaluated by comparisons with observed differential absorption LiDAR (DIAL) data (Su et al. 2017). In the DIAL technique, the mean gas concentration over a certain range interval is determined by analyzing the LiDAR backscatter signals for laser wavelengths tuned "on" (λ_{on}) and "off" (λ_{off}) in a molecular absorption peak of the gas under

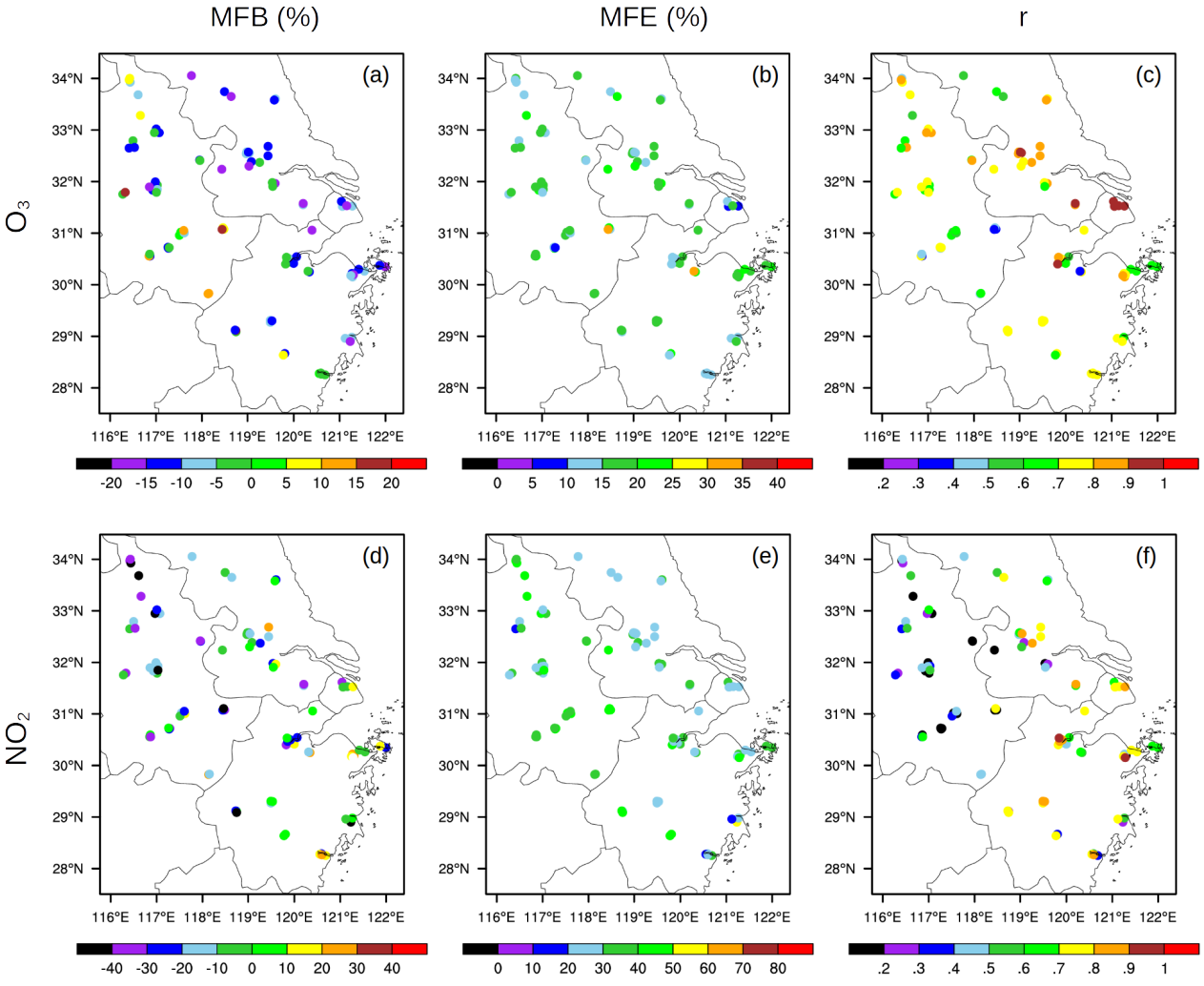

Fig. 2. Comparison of modeled air pollutant concentrations against measurements in 96 monitoring sites over YRD region during August 24–September 6, 2016: Mean fractional bias (MFB), mean fractional error (MFE) and Pearson's correlation coefficient (r) of O_3 (a–c) and NO_2 (d–f), respectively.

investigation (Browell et al., 1998). In the DIAL data of O_3, the vertical height available is from 0.3 km to 3 km due to the limitations of the signal-to-noise ratio and detection range.

3. Results

3.1. Model performance

We first evaluate the overall performance of WRF-Chem for the YRD region by incorporating data from the 96 air quality monitoring sites. Specifically, the maximum daily 8 h (MDA8) ozone and daily mean NO_2 concentrations at the surface are used. The spatial distributions of MFB and MFE for O_3 and NO_2 are illustrated in Fig. 2. In general, the model-simulated air pollutant concentrations agree well with the observations, with MFB and MFE for most of the sites meeting

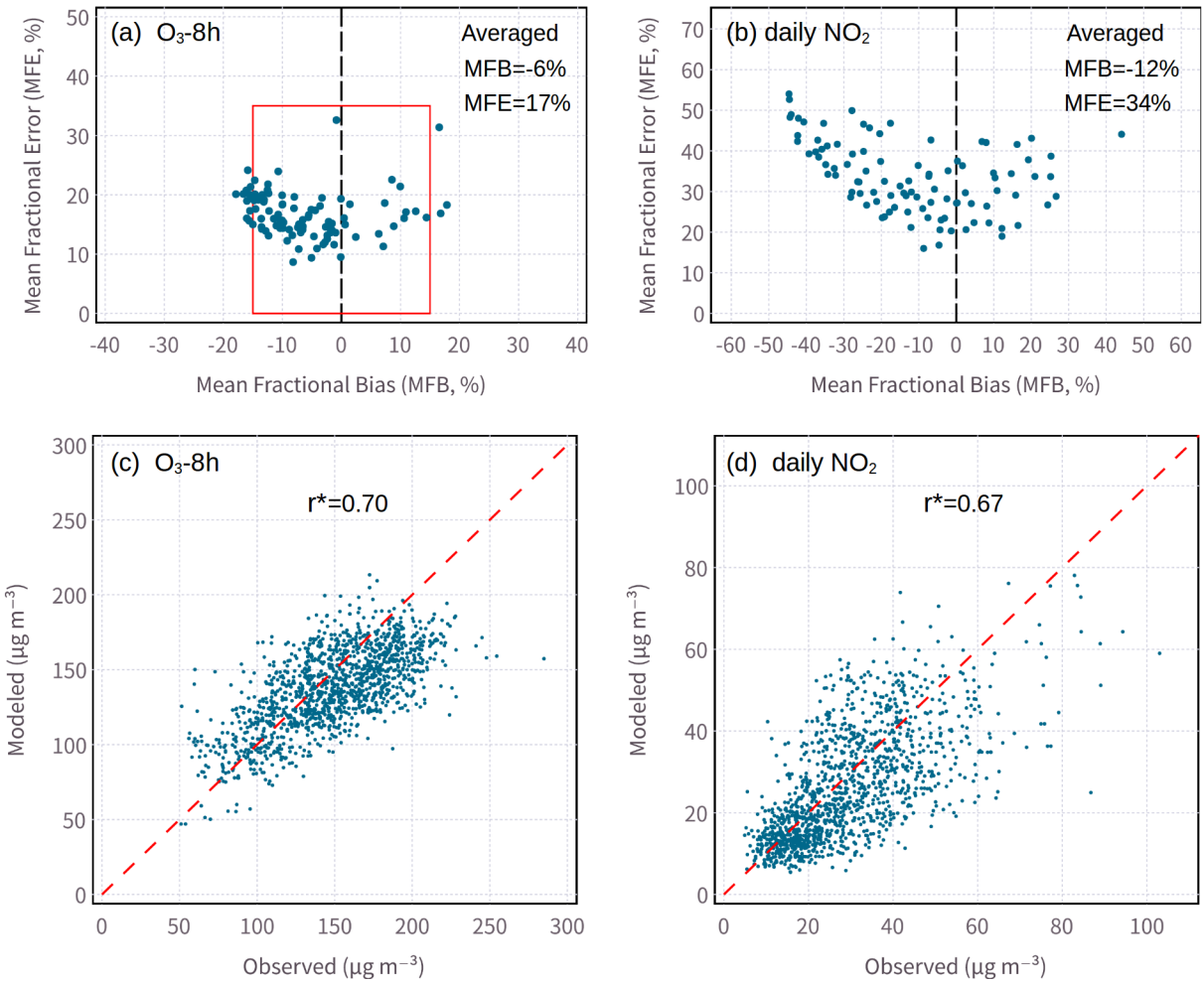

Fig. 3. Comparisons of modeled and observed concentrations of the air pollutants from 96 air quality monitoring sites across the YRD from 24 August to 06 September 2016 (1,344 pairs). Scatter plots for MFB and MFE of (a) O_3 and (b) NO_2. Performance goals (red box) for O_3 are the benchmarks. Scatter plots for daily observed and modeled (c) O_3 and (d) NO_2.

the benchmarks (MFB<15%; MFE<35%) (US EPA, 2007). A scatter plot of MFB/MFE is shown in Fig.3, further demonstrating the capability of the present model in reproducing the observations, which is also supported by the high correlation between model and observation (Fig. 3c, d).

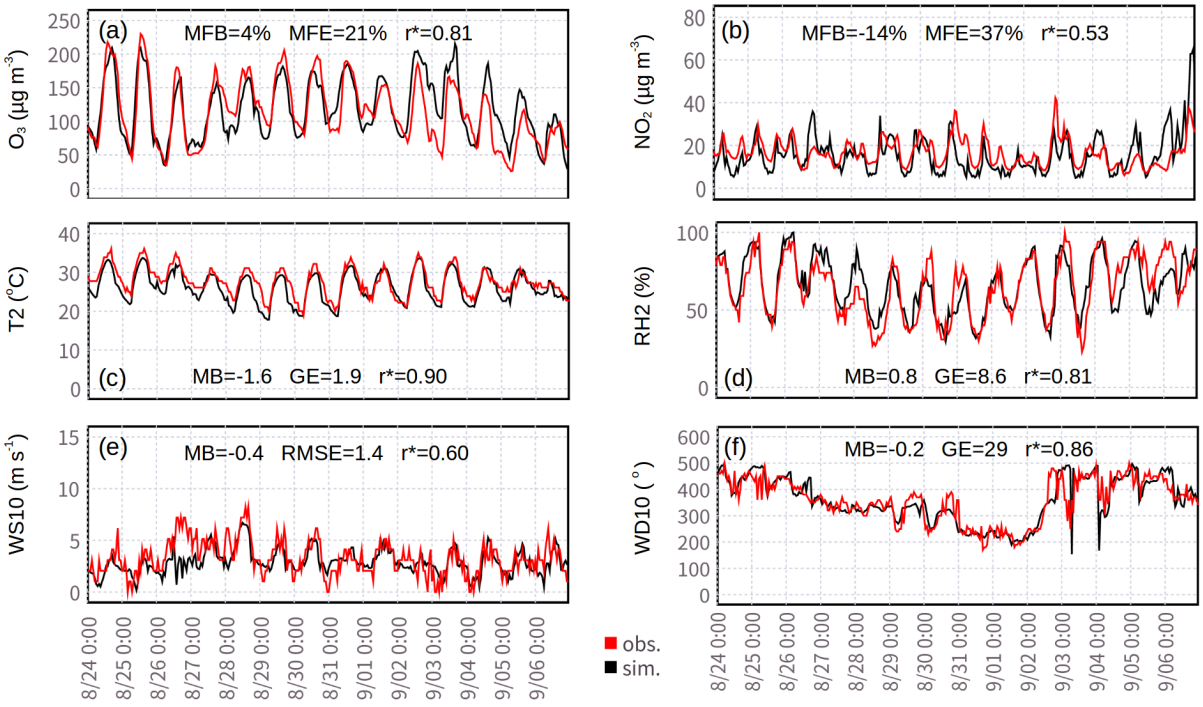

Fig. 4. Modeled air pollutants and meteorological parameters compared with measurements at the Hangzhou monitoring site from 24 August to 06 September 2016. Surface concentrations of (a) O_3 and (b) NO_2, (c) temperature at 2 m (T2), (d) relative humidity at 2 m (RH2), (e) wind speed at 10 m (WS10) and (f) wind direction at 10 m (WD10).

After the above overall evaluation of the present model in the whole YRD region, the site of Hangzhou will be focused on for further analysis. The time series of hourly simulated and observed air pollutants (O_3, Fig. 4a; NO_2, Fig. 4b) and meteorological factors (T2, Fig. 4c; RH2, Fig. 4d; WS10, Fig. 4e; and WD10, Fig. 4f) at Hangzhou are presented in Fig. 4. It is found that all modeled data are statistically significantly correlated with the observed data at the 95% level. The MFB and MFE for both O_3 and NO_2 are well below the benchmarks (MFB/MFE: 15%/35%; US EPA, 2007) and the observed diurnal variations are well reproduced. For meteorological parameters, $\leq \pm 0.5$°C, GE $\leq$ 2.0°C), 10 m wind speed (MB $\leq$ 0.5 m/s, RMSE $\leq$ 2.0 m/s) and 10 m wind direction (MB $\leq \pm 10°$, GE $\leq$ 30°). McNally (2009) suggested a relaxed benchmark for 2 m temperature (MB $\leq \pm 1.0$°C). In this study, the 10 m wind speed and wind direction (Fig. 3e, f) results are well within

the benchmarks. The GE of 2 m air temperature (1.9°C; Fig. 3c) also satisfies the criteria, but the MB is slightly higher (−1.6°C) which has also been noted in a previous study (Zhang et al., 2014). These comparisons further demonstrate that the present model is able to correctly predict the time series of both meteorological parameters and air pollutants of O_3 and NO_2 in Hangzhou.

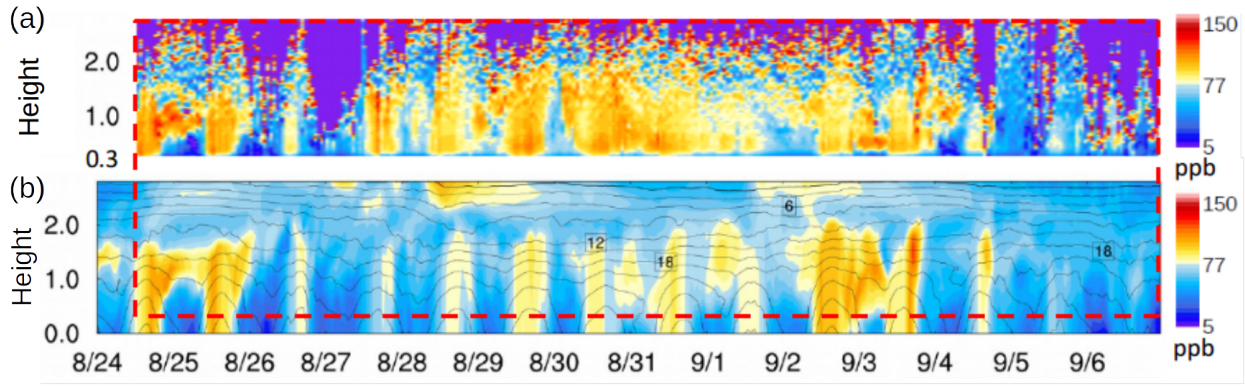

Fig. 5. Vertical comparison of hourly (a) observed (from differential absorption LiDAR) and (b) simulated O_3 concentrations (ppb) in Hangzhou from 24 August to 06 September 2016. Purple regions in the top panel denote invalid data with a low signal-to-noise ratio. To facilitate direct comparison, the red dashed line is added to indicate the ozone level recorded for the same time periods (starting from 12:00, 24 August) and vertical heights (0.3–3 km) in the observations and simulation results.

To further evaluate the capability of the model to predict the vertical structure of ozone concentration, the vertical distribution of the modeled O_3 in Hangzhou from 24 August to 06 September 2016 is qualitatively compared with the DIAL data, as shown in Fig. 5. It is interesting to find that the present model can successfully predict the spatial-temporal distribution of ozone in Hangzhou. All observed major features of ozone are well captured by the model. This gives us high confidence and lays a solid foundation for further exploring the pollution characteristics and influencing factors of ozone in Hangzhou during the G20 summit.

3.2. Spatial-temporal variations of O_3 pollution

To discuss spatial-temporal characteristics of O_3 pollution in Hangzhou, the whole emission control period can be divided into three stages according to the reduction intensity of the measures. August 24-27, 2016 is the first stage (S1) during which industrial and construction emission controls were implemented. During the second stage (S2, August 28-31), traffic restrictions were

263 further added. September 1-6 2016 is the third stage (S3) with the emergent VOCs control further
264 implemented. Figs. 4(a) and 4(b) in the above section also present the temporal evolution of O_3 and
265 its precursor NO_2 in Hangzhou city during the emission control period of G20 summit. It is evident
266 that the NO_2 has been significantly reduced by the emission control measures and the concentration
267 is well below the national level-II standard of 200 μg/m^3. However, the concentration of O_3 keeps
268 high levels for the whole 14 days, with 7 days of MDA8 are above and 4 days are close to the
269 national level-II standard (GB-3095–2012) of 160μg/m^3. This serious O_3 pollution indicates that the
270 emission control measures seem to make no obvious effect on ozone, which is consistent with
271 previous observations (Su et al. 2017; Wu et al. 2019). The diurnal variation of O_3 is similar for the
272

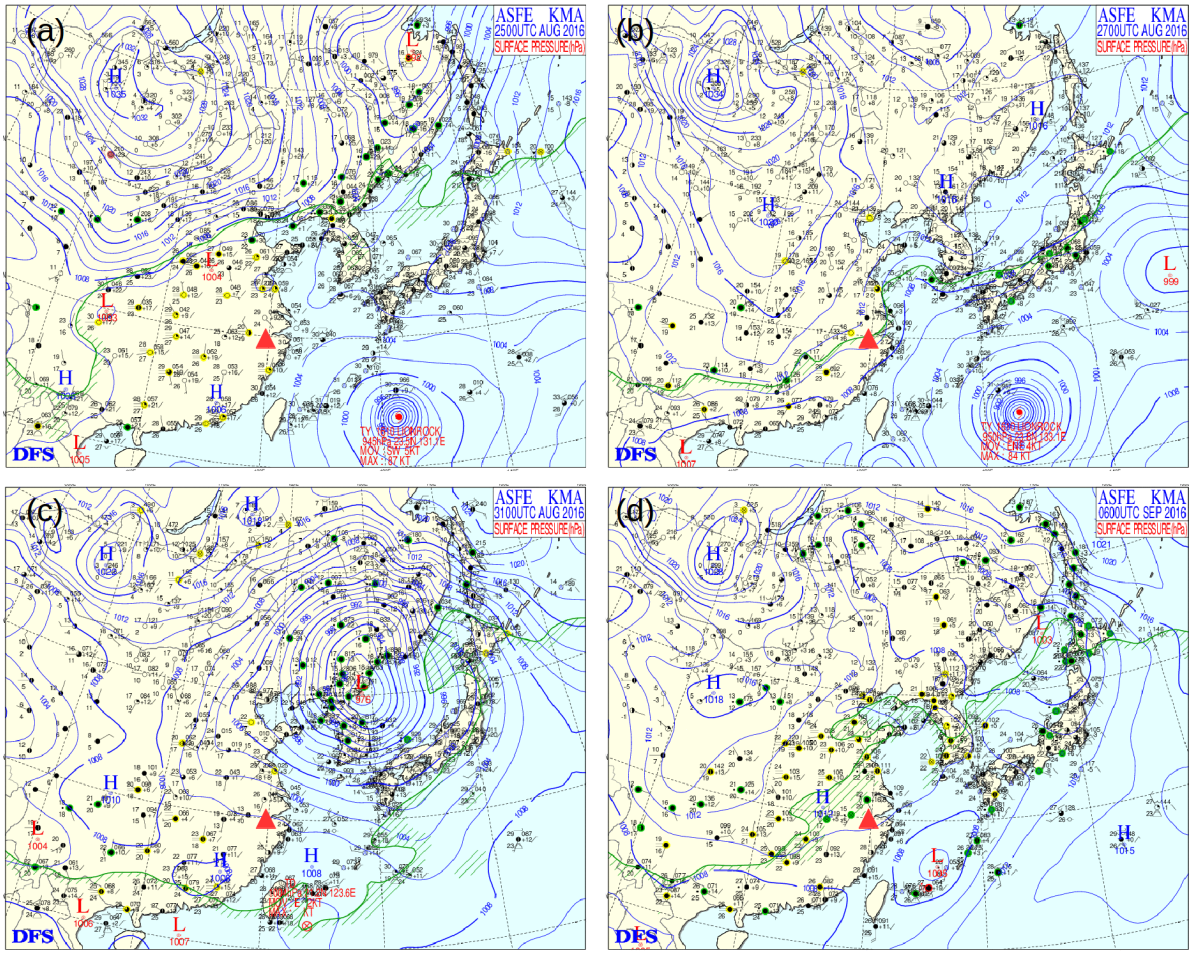

273 **Fig. 6.** Synoptic circulation in East Asia during the 2016 G20 summit. Weather charts for four representative
274 periods at 08:00 LST on (a) 25 August, (b) 27 August, (c) 31 August, and (d) 06 September 2016. LST: Local
275 Sidereal Time; H: High-pressure system; L: Low-pressure system. The red triangle denotes the location of
276 Hangzhou city.

three stages with a peak value at the time around 16:00 and a valley value at the time around 8:00 of each day. However, the variation magnitude in Stage 2 is obviously lower than those of other stages, which will be further discussed later.

Fig. 5 also clearly shows this diurnal variation of O_3 in the ground level. However, nocturnal O_3-rich mass is observed during certain periods in the upper air (approximately 1 km), such as August 25, August 31, and September 3, which makes an n-shaped distribution pattern of the O_3 in the upper air. This kind of spatial distribution of ozone will promote vertical exchange of O_3 in the area. In general, high concentrations of O_3 appear vertically until the top of the planetary boundary layer (PBL, approximately <2 km), suggesting the ozone pollution is not a local but a regional phenomenon in the whole low-level (from surface to close to the PBL height) region.

Considering the synoptic circulation is closely related to regional O_3 abundance, four representative surface weather charts obtained from the Korea Meteorological Administration are presented in Fig. 6. In the early stage, strong and uniform high-pressure fields covered vast regions of southeastern China, and a tropical cyclone moved northeastward over the East China Sea (Fig. 6a). In the middle stage (Fig. 6b), the tropical cyclone approached the YRD region, bringing strong north wind fields to this area. As a result, the long narrow rain band arrived in Hangzhou (red triangle) on 27 August 2016. In the later stage (Fig. 6c), the cyclone continuously moved and eventually hit the land, and the tropical high in the YRD region recovered gradually. Finally, the cyclone faded, and a rainstorm appeared over most of the YRD region (Fig. 6d).

The typical hourly vertical and horizontal O_3 distributions in the YRD region are further presented in Fig.7. The wind fields are also included for better understanding. For stagnation days with weak wind fields and strong radiation before or after the tropical cyclone, meteorological conditions are unfavorable for pollutant dispersion. As a result, O_3 pollution is more regional and intense, with an hourly peak O_3 concentration of 250 $\mu g/m^3$ appeared within the planetary boundary layer in the whole YRD region, as shown in Figs. 7a and 7c. In these conditions, photochemical

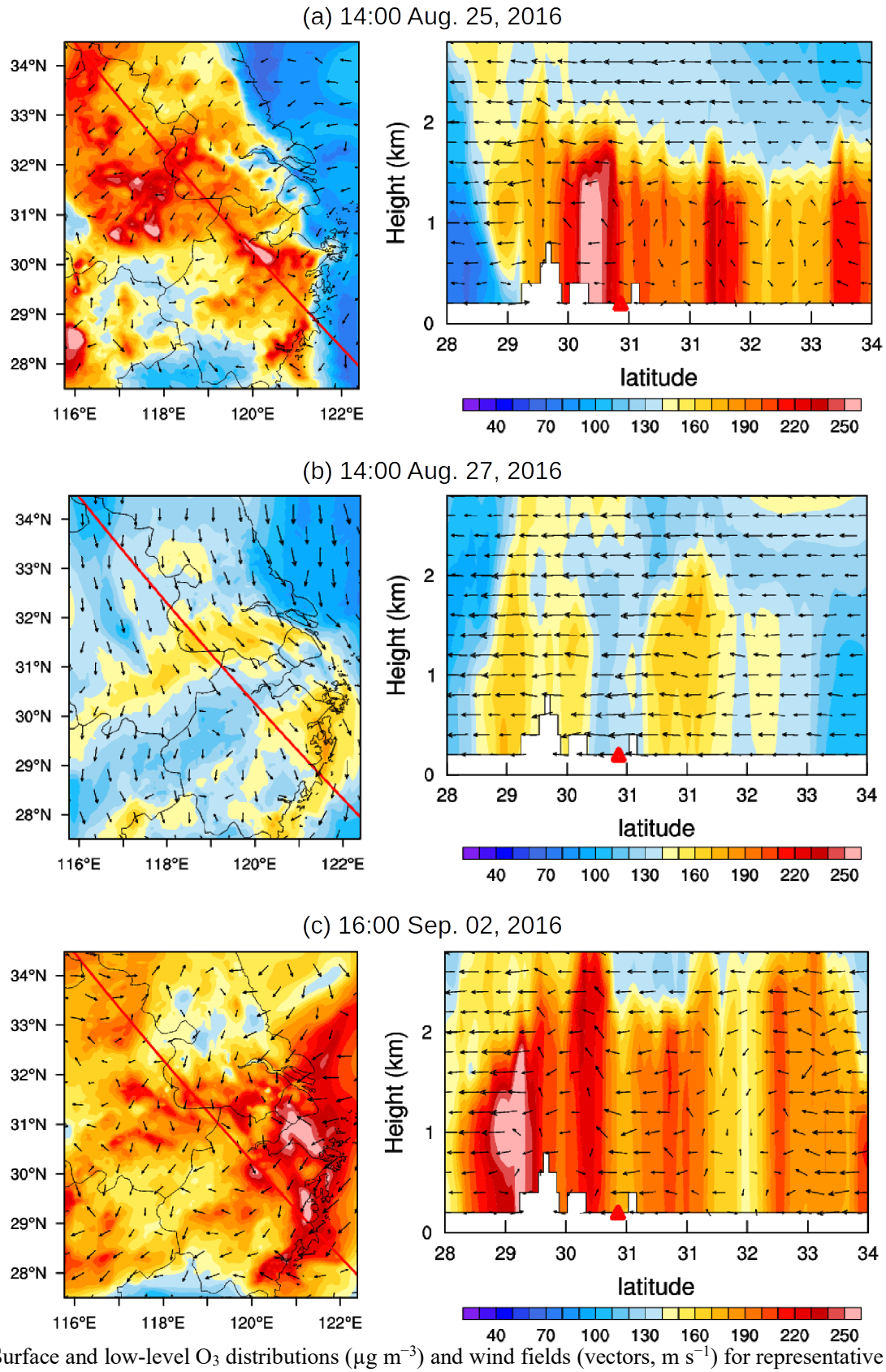

Fig. 7. Surface and low-level O_3 distributions (μg m^{-3}) and wind fields (vectors, m s^{-1}) for representative episodes. (a) Stagnant weather before the tropical cyclone, (b) pollutant transport when the tropical cyclone approached, and (c) stagnant weather after the cyclone. The red line denotes the cross-section line of low-level O_3 distributions. The red triangle denotes the location of Hangzhou.

reactions dominate the ozone formation and accumulation. This phenomenon is consistent with the satellite-derived tropospheric O_3 distribution in the area (Su et al. 2017), and is also supported by the observed ozone data from the 96 sites in the YRD region as shown in Fig. 3c. During the 14-day emission control period of G20 summit, 52% of the observed ozone samples from the 96 sites are above the China's national level-II standard (160μg/m^3), suggesting that regional ozone pollution appears in the YRD region during the study period. As the cyclone approached on 27 August, a large belt of O_3 mass appeared in the upwind direction and moved toward Hangzhou under a prevailing north wind field (Fig. 7b). Regional pollutant transport may play an important role under this condition. However, because of the rain and cooling effects from the cyclone, the ozone concentration is relatively low in the whole YRD region.

3.3. Process analysis of O_3 formation

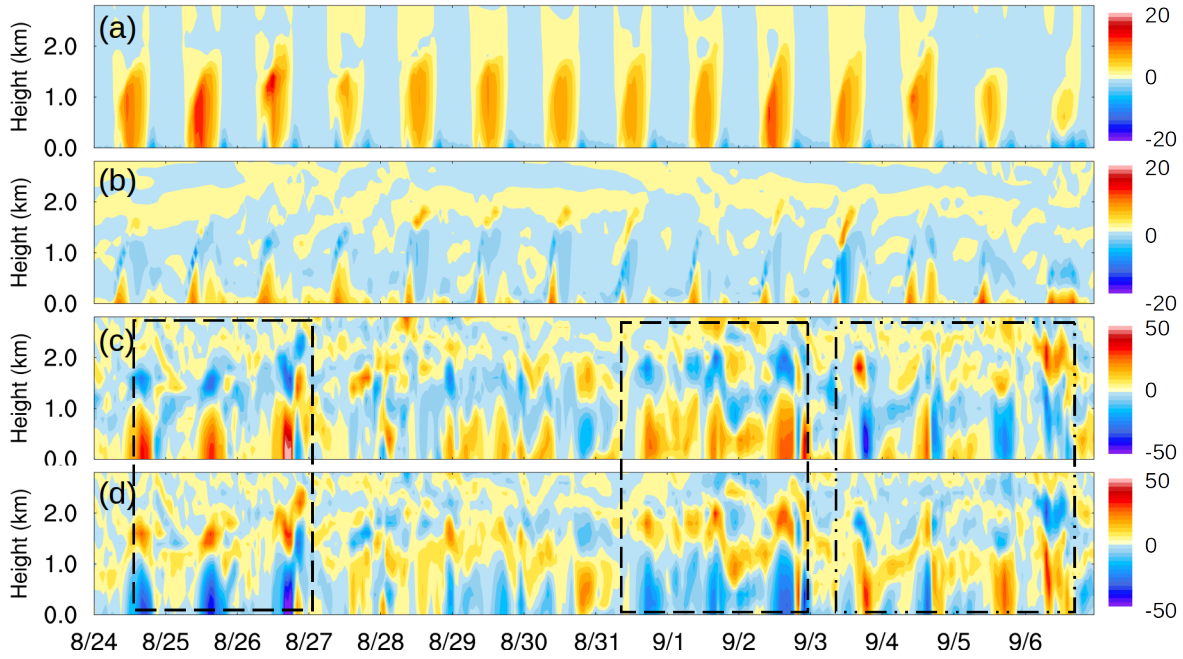

Fig. 8. Hourly variations in the change rate of low-level O_3 (ppb h^{-1}) resulted from (a) gas chemistry, (b) vertical diffusion, (c) horizontal advection, and (d) vertical advection in Hangzhou.

To further investigate the underlying mechanism of O_3 pollution, hourly variations in the change rate of low-level O_3 resulting from different physical and chemical processes are presented in Fig.8. It is evident that gas chemistry is the dominant factor to the strong generation of abundant O_3 in the entire planetary boundary layer (<2 km) in the daytime but causes small amount of

depletion of O_3 at the near-surface height (<0.3 km) in the nighttime (Fig. 8a). High concentration of O_3 diffuses from the upper layer downward to the ground through vertical diffusion during the whole study period, which is obvious in the daytime (Fig. 8b). However, this effect is relatively weak compared to other processes. Horizontal and vertical advections seem to play more important roles in shaping the near-surface O_3, as indicated in Figs. 8c and 8d. Several interesting dynamic O_3 circulations are observed between the near-surface and upper-air regions and indicated by the dashed boxes. During the periods of 24-26 August and 31 August to 2 September 2016, O_3-rich mass in the lower layer (<1 km) travels to Hangzhou through horizontal advection, and is then transported upward to the higher layer through vertical advection. At this higher layer, the mass

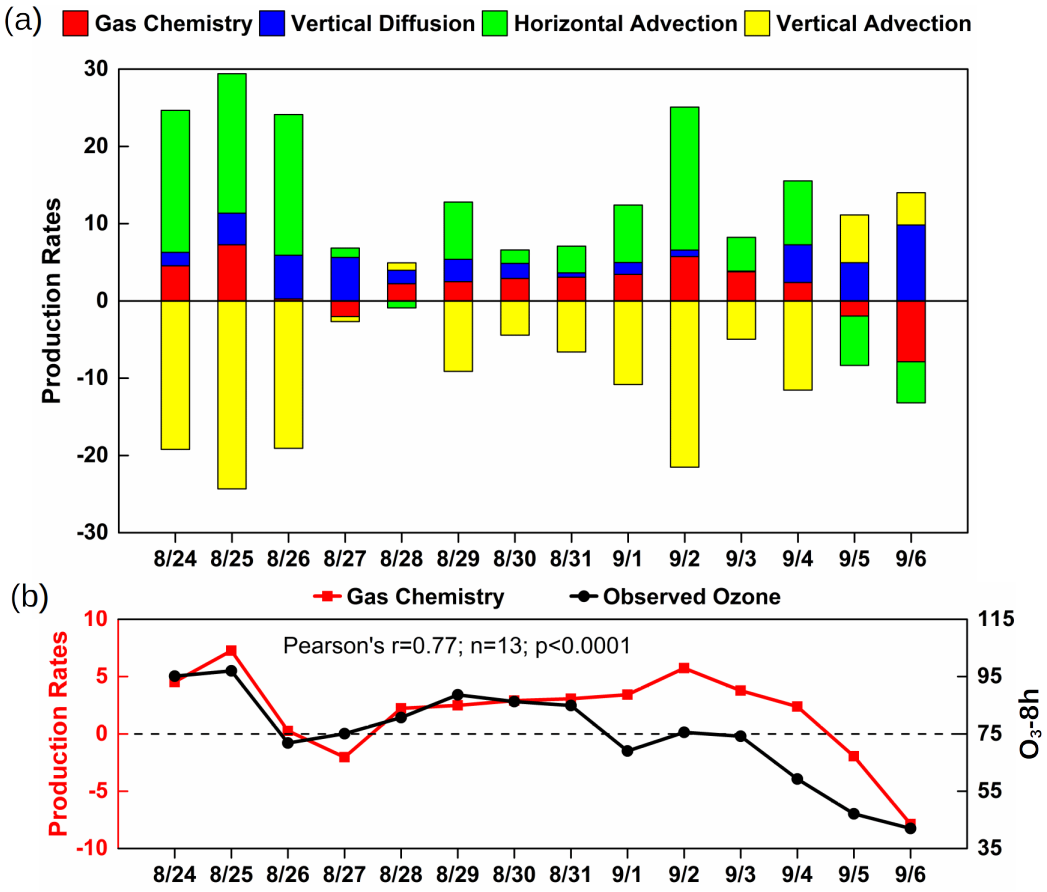

Fig. 9. (a) Daytime mean (08:00–17:00 LST) change rate of simulated surface O_3 (ppb h^{-1}; left *y* axis) resulted from gas chemistry, vertical diffusion, horizontal and vertical advections in Hangzhou. (b) Correlation of daytime mean gas chemistry generation (ppb h^{-1}; left *y* axis) and observed surface-level maximum for daily 8h concentration of O_3 (ppb; right *y* axis) in Hangzhou. China's national level-II standard is approximately 75 ppb (160 μg m^{-3}).

subsequently travels away from Hangzhou to other places through horizontal advection in a circular manner. This phenomenon might be associated with the urban heat island circulation (Lai and Cheng, 2009). However, during the period of September 3-6 2016, similar circulation phenomenon is observed, but the flow direction is reverse. The O_3-rich mass travels downward to the ground through vertical advection and is then transported to surrounding regions through horizontal advection. This downward circulation is also related to the meteorological conditions after the cyclone. In addition, the horizontal and vertical advections of O_3 take on a chaotic status during August 27-30, 2016, suggesting that complicated variable meteorological conditions happened in the time. This is also the reason for the lower magnitude of diurnal variation in Stage 2.

Fig. 9 shows the daytime mean change rate of simulated O_3 at the ground level resulted from various atmospheric processes and the correlation of gas chemistry generation and observed maximum for daily 8h concentration of O_3. As a whole, the main sources of local surface ozone in Hangzhou are from gas chemistry, vertical diffusion, and horizontal advection, with mean production rates of 1.9, 3.3, and 6.7 ppb h^{-1}, respectively, from August 24 to September 6, 2016, and the major sink is vertical advection. However, during some days such as September 5-6, the gas chemistry consumes O_3 while the vertical advection increases it. In general, strong net horizontal and vertical advections of O_3 are observed for most days of the period, except August 27-28 during

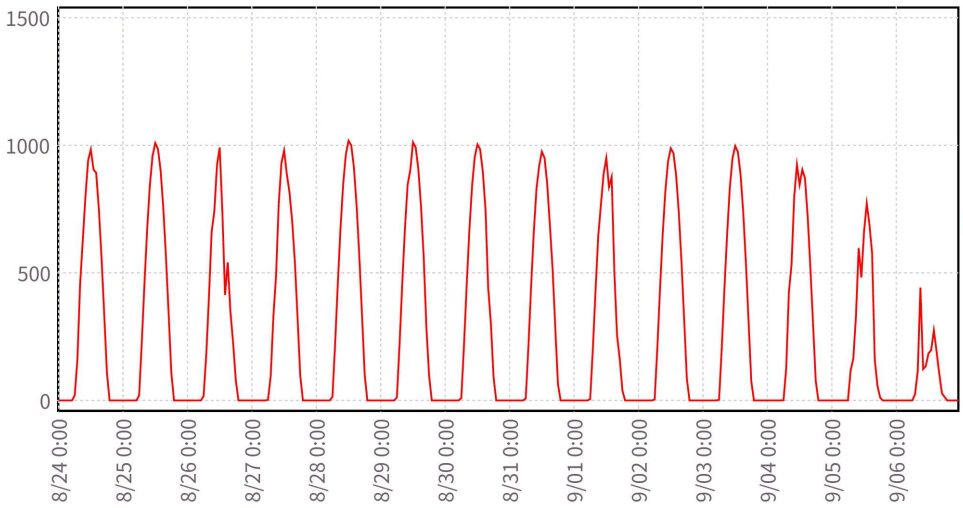

Fig. 10. Simulated hourly downward short wave flux at ground surface in Hangzhou (W m^{-2}) during August 24 to September 6, 2016.

360 which the strongest northwest cold winds (Fig. 4e) occurred and made the net advections of O_3
361 negligible. Similar to Fig. 8, dynamic O_3 circulations are observed for the periods of August 24-26,
362 August 31 to September 2, and September 5-6. Particularly, the circular direction is reverse during
363 September 5-6 and the net gas chemistry is to consume ozone due to weak solar radiation in the
364 days as shown in Fig. 10.

365 In addition, the variation trend of the daytime mean production rate of gas chemistry is
366 consistent with the observed MDA8 concentration and the local chemical generation has large
367 positive correlation (Pearson's r = 0.77) with the observed MDA8 concentrations (Fig. 8b). This
368 indicates a trade-off effect among vertical diffusion, horizontal advection, and vertical advection.
369 High O_3 concentrations (i.e., 25 August 2016 MDA8: 98 ppb) are always accompanied by strong
370 radiation and prolific generation of gas chemical reactions. It is also interesting to find that vertical
371 diffusion may partially compensate for gas chemistry when the chemical reaction rate is relatively
372 low or negative. For example, during August 26-27 and September 5-6, the vertical diffusion rates
373 are higher than the chemical production rates. The low O_3 episode on these periods may result from
374 local chemical consumption.

375 ## 4. Discussion

376 The above results demonstrate that high ozone concentrations are observed, temporarily during
377 most day time of the emission control period of G20 summit, and spatially in Hangzhou and even
378 the whole YRD region, from the surface to the top of the planetary boundary layer. Strong
379 horizontal and vertical advections appear, but they form circulations due to special meteorological
380 conditions so that the effects of them almost cancel each other out. As a result, the serious ozone
381 pollution in Hangzhou is mainly resultant from the local photochemical reactions. When the
382 photochemical reactions are weak, the vertical diffusion from the upper-air notable background O_3
383 further compensates for the local surface ozone concentration. Therefore, it is of great importance to
384 understand why the strict emission control measures make no obvious effect on the local
385 photochemical reactions of ozone generation.

Chemical generation of O_3 is the net effect of photochemical generation and titration consumption. VOC oxidation (Jenkin et al., 1997; Sillman, 1999) in photochemical reactions provides critical oxidants (i.e., RO_2) that efficiently convert NO to NO_2, resulting in further accumulation of O_3 (Wang et al., 2017). The chemical generation of O3 is controlled by NO_x and VOCs depending on which substance is lack in the reactions. As a consequence, there are two sensitivity regimes of O_3 production, namely, the NO_x-limited and VOC-limited regimes. Previous studies have shown that the sensitivity pattern of surface O_3 formation in Hangzhou is dominant by the VOCs-limited regime (Yan *et al.* 2016; Li *et al.*, 2017; Su *et al.*, 2017). In this regime, if the regional reduction of VOCs is much higher than that of NO_x, the O_3 concentration can be reduced, otherwise if the regional reduction of VOCs is much less than that of NO_x, the inhibitory effect of NO_x on O_3 generation will be weakened, and the O_3 concentration will increase remarkably (Wang et al. 2015). According to the studies of Su et al. (2017), Zheng et al. (2019), and Wu et al. (2019), it can be deduced that NO_x has been significantly reduced by about 60%, at least two times of the reduction of VOCs in Hangzhou. The influence of stringent emission control measures on VOCs is not as immediate and effect as that on NO_x, which is associated with the fact that there was a large amount of biogenic VOC emission in Hangzhou and surrounding regions (Liu et al. 2018; Wu et al. 2020). In fact, the average temperature during the study period is as high as around 31°C (Fig. 4c), which facilitates the biogenic VOC emissions and photochemical reactions. As a result, the photochemical generation of O_3 was not under control and high concentration of ozone appeared. However, it is worth noting that after the emergent VOCs control measures had been implemented in the area during the third stage, the net generation rate of O_3 gradually reduces since September 2, 2016, leading to a period of relatively low ozone concentration together with other meteorological effects. These discussions implicate that to alleviate ozone pollution, the ratio of reduction of VOCs to that of NO_x is the key parameter based on the O_3-NO_x-VOCs sensitivity analysis. As the biogenic VOCs are important sources of the total VOCs in the YRD region, it is necessary to balance the reduction of NO_x to make the ratio within effective regime in the future.

5. Conclusions

To understand the unique response of ozone to short-term emission control measures during the G20 summit in Hangzhou, the spatial-temporal characteristics and process analysis of O_3 pollution are investigated by using the WRF-Chem model. Statistical evaluations of meteorological and chemical parameters suggest that the model system is able to reasonably predict the observed data for both the ground and upper-air levels in MICS-Asia III. High ozone concentrations are observed, temporarily during most day time of the emission control period of G20 summit, and spatially in Hangzhou and even the whole YRD region, from the surface to the top of the planetary boundary layer. Horizontal and vertical advection circulations are captured in Hangzhou, with horizontal advection the source and vertical advection the sink of the surface O_3 in Hangzhou. Consequently, the serious ozone pollution is mainly resultant from the local photochemical reactions which are not under good control by the emission reduction measures. As the surface O_3 formation in Hangzhou is dominant by the VOCs-limited regime, the significant reduction of NO_x compared to that of VOCs is unfavorable to chemical generation of O_3. The ratio of reduction of VOCs to that of NO_x based on the O_3-NO_x-VOCs sensitivity analysis is a critical parameter for reduction of ozone formation from photochemical reactions. In addition, it is found that the vertical diffusion from the upper-air notable background O_3 also plays an important role in shaping the surface ozone concentration when the photochemical reactions are weak.

Author contribution

Zhizhen Ni: Data curation, Investigation, Writing - original draft. **Kun Luo:** Methodology, Resources, Writing - review & editing, Supervision. **Yang Gao:** Formal analysis, Methodology, Writing - review & editing. **Xiang Gao:** Data curation, Resources. **Fei Jiang:** Methodology, Writing - review & editing. **Cheng Huang:** Data curation, Formal analysis. **Jianren Fan:** Resources, Supervision. **Joshua Fu**: Writing - review & editing. **Changhong Chen**: Formal analysis.

Acknowledgments

This work was financially supported by special funds from the Ministry of Environmental Protection of China (No. 201409008-4) and the Zhejiang Provincial Key Science and Technology Project for Social Development (No. 2014C03025). We would like to thank the US National Oceanic and Atmospheric Administration for its technical support in WRF-Chem modeling. High-resolution emission inventories were provided by the Institute of Environmental Science, Shanghai, China, and the official documents of emission control policies were obtained from the Hangzhou Environmental Monitoring Center.

Competing interests

The authors declare that they have no conflict of interest.

References

Browell, E.V., Ismail, S., Grant, W.B.: Differential absorption lidar (DIAL) measurements from air and space, Appl. Phys. B Lasers Opt, 67, 399–410, https://doi.org/10.1007/s003400050523, 1998.

Browell, E. V.: Differential Absorption Lidar Sensing of Ozone, Proc. IEEE, 77, 419–432, https://doi.org/10.1109/5.24128, 1989

Brown, J.F., Loveland, T.R., Merchant, J.W., Reed, B.C., Ohlen, D.O.: Using Multisource Data in Global Land-Cover Characterization - Concepts, Requirements, and Methods, Photogramm. Eng. Remote Sensing, 59, 977–987, 1993.

Calfapietra, C., Morani, A., Sgrigna, G., Di Giovanni, S., Muzzini, V., Pallozzi, E., Guidolotti, G., Nowak, D., Fares, S.: Removal of Ozone by Urban and Peri-Urban Forests: Evidence from Laboratory, Field, and Modeling Approaches, J. Environ. Qual, 45, 224, https://doi.org/10.2134/jeq2015.01.0061, 2016.

Cheng, W.L., Lai, L.W., Den, W., Wu, M.T., Hsueh, C.A., Lin, P.L., Pai, C.L., Yan, Y.L.: The relationship between typhoons' peripheral circulation and ground-level ozone concentrations in central Taiwan, Environ. Monit. Assess, 186, 791–804, https://doi.org/10.1007/s10661-013-3417-7, 2014.

Emery, C., Tai, E., Yarwood, G.: Enhanced meteorological modeling and performance evaluation for two Texas episodes, International Corp (Ed.), Report to the Texas Natural Resources Conservation Commission, p.b.E (2001) [Novato, CA.], 2001

Emmons, L.K., Walters, S., Hess, P.G., Lamarque, J.-F., Pfister, G.G., Fillmore, D., Granier, C., Guenther, A., Kinnison, D., Laepple, T., Orlando, J., Tie, X., Tyndall, G., Wiedinmyer, C., Baughcum, S.L., Kloster, S.: Description and evaluation of the Model for Ozone and Related chemical Tracers, version 4 (MOZART-4), Geosci. Model Dev., 3, 43–67, https://doi.org/10.5194/gmd-3-43-2010, 2010.

Friedl, M. ., McIver, D. ., Hodges, J. C. ., Zhang, X. ., Muchoney, D., Strahler, A. ., Woodcock, C. ., Gopal, S., Schneider, A., Cooper, A., Baccini, A., Gao, F. and Schaaf, C.: Global land cover mapping from MODIS: algorithms and early results, Remote Sens. Environ., 83(12), 287–302, https://doi.org/10.1016/S0034-4257(02)00078-0, 2002.

Gao, J., Zhu, B., Xiao, H., Kang, H., Hou, X., Shao, P.: A case study of surface ozone source apportionment during a high concentration episode, under frequent shifting wind conditions over the Yangtze River Delta, China, Sci. Total Environ, 544, 853–863, https://doi.org/10.1016/j.scitotenv.2015.12.039, 2016.

Gonçalves, M., Jiménez-Guerrero, P., Baldasano J.M.: Contribution of atmospheric processes affecting the dynamics of air pollution in South-Western Europe during a typical summertime photochemical episode, Atmos. Chem. Phys, 9, 849–864, https://doi.org/10.5194/acp-9-849-2009, 2009.

Grell, G.A., Peckham, S.E., Schmitz, R., McKeen, S.A., Frost, G., Skamarock, W.C., Eder, B. Fully coupled "online" chemistry within the WRF model, Atmos. Environ., 39, 6957–6975, https://doi.org/10.1016/j.atmosenv.2005.04.027, 2005.

Grell, G., Baklanov, A.: Integrated modeling for forecasting weather and air quality: A call for fully coupled approaches, Atmos. Environ., 45, 6845–6851, https://doi.org/10.1016/j.atmosenv.2011.01.017, 2011.

Haiwei Li, Dongfang Wang, Long Cui, Yuan Gao, Juntao Huo, Xinning Wang, Zhuozhi Zhang, Yan Tan, Yu Huang, Junji Cao, Judith C. Chow, Shun-cheng Lee, Qingyan Fu. Characteristics of atmospheric PM2.5 composition during the implementation of stringent pollution control measures in shanghai for the 2016 G20 summit. Science of the Total Environment 648 (2019) 1121?1129

Ha, S., Hu, H., Roussos-Ross, D., Haidong, K., Roth, J., Xu, X.: The effects of air pollution on adverse birth outcomes, Environ. Res., 134, 198–204, https://doi.org/10.1016/j.envres.2014.08.002, 2014.

Huang, J.P., Fung, J.C.H., Lau, A.K.H., Qin, Y.: Numerical simulation and process analysis of typhoon-related ozone episodes in Hong Kong, J. Geophys. Res. D Atmos., 110, 1–17, https://doi.org/10.1029/2004JD004914, 2005.

Huang, C., Chen, C. H., Li, L., Cheng, Z., Wang, H. L., Huang, H. Y., Streets, D. G., Wang, Y. J., Zhang, G. F. and Chen, Y. R.: Emission inventory of anthropogenic air pollutants and VOC species in the Yangtze River Delta region, China, Atmos. Chem. Phys., https://doi.org/10.5194/acp-11-4105-2011, 2011.

Huan Yu, Wei Dai, Lili Ren, Dan Liu, Xintian Yan, Hang Xiao, Jun He, Honghui Xu. The Effect of Emission Control on the Submicron Particulate Matter Size Distribution in Hangzhou during the 2016 G20 Summit. Aerosol and Air Quality Research, 18: 2038–2046, 2018.

Hung, C.H., LouoC, K.: Relationships between Ambient Ozone Concentration Changes in Southwestern Taiwan and Invasion Tracks of Tropical Typhoons, Adv. Meteorol., https://doi.org/10.1155/2015/402976, 2015.

Hu S.W., Wu, X.F., Luo K., Gao, X. and Fan, J.R. (2015). Source apportionment of air pollution in Hangzhou city based on CMAQ. Energy Eng. 7: 40–44.

Jenkin, M. E., Saunders, S. M. and Pilling, M. J.: The tropospheric degradation of volatile organic compounds: A protocol for mechanism development, Atmos. Environ., 31(1), 81–104, https://doi.org/10.1016/S1352-2310(96)00105-7, 1997.

Jfffries H. E., Tonnesen S.: A comparison of two photochemical reaction mechanisms using mass balance and process analysis, Atmospheric Environment, 28(18), 2991-3003, 1994.

Jiang, F., Zhou, P., Liu, Q., Wang, T., Zhuang, B., Wang, X.: Modeling tropospheric ozone formation over East China in springtime, J. Atmos. Chem., 69, 303–319, https://doi.org/10.1007/s10874-012-9244-3, 2012.

Jiang, Y.C., Zhao, T.L., Liu, J., Xu, X.D., Tan, C.H., Cheng, X.H., Bi, X.Y., Gan, J.B., You, J.F., Zhao, S.Z.: Why does surface ozone peak before a typhoon landing in southeast China?, Atmos. Chem. Phys., 15, 13331–13338, https://doi.org/10.5194/acp-15-13331-2015, 2015.

Ji, Y., Qin, X., Wang, B., Xu, J., Shen, J., Chen, J., Huang, K., Deng, C., Yan, R., Xu, K. and Zhang, T. (2018). Counteractive effects of regional transport and emission control on the formation of fine particles: A case study during the Hangzhou G20 summit. Atmos. Chem. Phys. 18: 13581–13600.

Jones, S.L., Creighton, G.A., Kuchera, E.L., Rentschler, S.A.: Adapting WRF-CHEM GOCART for Fine-Scale Dust Forecasting, in: AGU Fall Meeting Abstracts, p. 6., 2011.

Kai Wu, Ping Kang, Xin Tie, Shan Gu, Xiaoling Zhang, Xiaohang Wen, Lingkai Kong, Sihui Wang, Yuzi Chen, Weihao Pan, Zhanshan Wang. Evolution and Assessment of the Atmospheric Composition in Hangzhou and its Surrounding Areas during the G20 Summit. Aerosol and Air Quality Research, 19: 2757–2769, 2019

Kalnay, E., M. Kanamitsu, R. Kistler, W. Collins, D. Deaven, L. Gandin, M. Iredell, S. Saha, G. White, J. Woollen, Y. Zhu, M. Chelliah, W. Ebisuzaki, W. Higgins, J. Janowiak, K.C. Mo, C. Ropelewski, J. Wang, A. Leetmaa,

R. Reynolds, R. Jenne, and D. Joseph: The NCEP/NCAR 40-Year Reanalysis Project, Bull. Amer. Meteor. Soc., 77, 437–472, https://doi.org/10.1175/1520-0477(1996)077<0437:TNYRP>2.0.CO;2, 1996.

Kheirbek, I., Wheeler, K., Walters, S., Kass, D., Matte, T.: PM2.5 and ozone health impacts and disparities in New York City: Sensitivity to spatial and temporal resolution, Air Qual. Atmos. Heal., 6, 473–486, https://doi.org/10.1007/s11869-012-0185-4, 2013.

Knote, C., Tuccella, P., Curci, G., Emmons, L., Orlando, J.J., Madronich, S., Baró, R., Jiménez-Guerrero, P., Luecken, D., Hogrefe, C., Forkel, R., Werhahn, J., Hirtl, M., Pérez, J.L., San José, R., Giordano, L., Brunner, D., Yahya, K., Zhang, Y.: Influence of the choice of gas-phase mechanism on predictions of key gaseous pollutants during the AQMEII phase-2 intercomparison, Atmos. Environ., 115, 553–568, https://doi.org/10.1016/j.atmosenv.2014.11.066, 2015.

Lai, L. W. and Cheng, W. L.: Air quality influenced by urban heat island coupled with synoptic weather patterns, Sci. Total Environ., 407(8), 2724–2733, https://doi.org/10.1016/j.scitotenv.2008.12.002, 2009.

Landry, J.S., Neilson, E.T., Kurz, W.A., Percy, K.E.: The impact of tropospheric ozone on landscape-level merchantable biomass and ecosystem carbon in Canadian forests, Eur. J. For. Res., 132, 71–81, https://doi.org/10.1007/s10342-012-0656-z, 2013.

Li, J., Nagashima, T., Kong, L., Ge, B., Yamaji, K., Fu, J. S., Wang, X., Fan, Q., Itahashi, S., Lee, H.-J., Kim, C.-H., Lin, C.-Y., Zhang, M., Tao, Z., Kajino, M., Liao, H., Li, M., Woo, J.-H., Kurokawa, J.-I., Wu, Q., Akimoto, H., Carmichael, G. R., and Wang, Z.: Model evaluation and inter-comparison of surface-level ozone and relevant species in East Asia in the context of MICS-Asia phase III Part I: overview, Atmos. Chem. Phys. Discuss., https://doi.org/10.5194/acp-2018-1283, in review, 2019.

Li, K., Chen, L., Ying, F., White, S.J., Jang, C., Wu, X., Gao, X., Hong, S., Shen, J., Azzi, M. and Cen, K. (2017). Meteorological and chemical impacts on ozone formation: A case study in Hangzhou, China. Atmos. Res. 196: 40–52.

Li, L., Chen, C. H., Fu, J. S., Huang, C., Streets, D. G., Huang, H. Y., Zhang, G. F., Wang, Y. J., Jang, C. J., Wang, H. L., Chen, Y. R. and Fu, J. M.: Air quality and emissions in the Yangtze River Delta, China, Atmos. Chem. Phys., https://doi.org/10.5194/acp-11-1621-2011, 2011.

Li, M., Song, Y., Huang, X., Li, J., Mao, Y., Zhu, T., Cai, X. and Liu, B.: Improving mesoscale modeling using satellite-derived land surface parameters in the Pearl River Delta region, China, J. Geophys. Res. Atmos., 119(11), 6325–6346, https://doi.org/10.1002/2014JD021871, 2014.

Li, M., Zhang, Q., Kurokawa, J.-I., Woo, J.-H., He, K., Lu, Z., Ohara, T., Song, Y., Streets, D.G., Carmichael, G.R., Cheng, Y., Hong, C., Huo, H., Jiang, X., Kang, S., Liu, F., Su, H., Zheng, B.: MIX: a mosaic Asian anthropogenic emission inventory under the international collaboration framework of the MICS-Asia and HTAP, Atmos. Chem. Phys., 17, 935–963, https://doi.org/10.5194/acp-17-935-2017, 2017.

Lin, M., Fiore, A.M., Cooper, O.R., Horowitz, L.W., Langford, A.O., Levy, H., Johnson, B.J., Naik, V., Oltmans, S.J., Senff, C.J.: Springtime high surface ozone events over the western United States: Quantifying the role of stratospheric intrusions, J. Geophys. Res. Atmos., 117, https://doi.org/10.1029/2012JD018151, 2012.

Lin, M., Fiore, A.M., Horowitz, L.W., Langford, A.O., Oltmans, S.J., Tarasick, D., Rieder, H.E.: Climate variability modulates western US ozone air quality in spring via deep stratospheric intrusions, Nat. Commun., 6, 7105, https://doi.org/10.1038/ncomms8105, 2015.

Liu, H., Ma, W., Qian, J., Cai, J., Ye, X., Li, J. and Wang, X. (2015). Effect of urbanization on the urban meteorology and air pollution in Hangzhou. J. Meteorol. Res. 29: 950–965.

Liu, Y., Li, L., An, J., Huang, L., Yan, R., Huang, C., Wang, H., Wang, Q., Wang, M. and Zhang, W.: Estimation of biogenic VOC emissions and its impact on ozone formation over the Yangtze River Delta region, China, Atmos. Environ., https://doi.org/10.1016/j.atmosenv.2018.05.027, 2018.

McNally DE: 12 km MM5 performance goals, Presentation to the Ad-hov Meteorology Group, 2009.

Monks, P.S., Archibald, A.T., Colette, A., Cooper, O., Coyle, M., Derwent, R., Fowler, D., Granier, C., Law, K.S., Mills, G.E., Stevenson, D.S., Tarasova, O., Thouret, V., von Schneidemesser, E., Sommariva, R., Wild, O., Williams, M.L.: Tropospheric ozone and its precursors from the urban to the global scale from air quality to short-lived climate forcer, Atmos. Chem. Phys., 15, 8889–8973, https://doi.org/10.5194/acp-15-8889-2015, 2015.

Nagashima, T., Sudo, K., Akimoto, H., Kurokawa, J., Ohara, T., 2017. Long-term change in the source contribution to surface ozone over Japan. Atmos. Chem. Phys. 17, 8231–8246, https://doi.org/10.5194/acp-17-8231-2017

Ni, Z. zhen, Luo, K., Zhang, J. xi, Feng, R., Zheng, H. xin, Zhu, H. ran, Wang, J. fan, Fan, J. ren, Gao, X. and Cen, K. fa: Assessment of winter air pollution episodes using long-range transport modeling in Hangzhou, China, during World Internet Conference, 2015, in Environmental Pollution, vol. 236, pp. 550–561., 2018.

Ni, Z. zhen, Luo, K., Gao, X., Gao, Y., Fan, J. ren, Fu, Joshua S. Cen, C.,: Exploring the stratospheric source of ozone pollution over China during the 2016 Group of Twenty summit, 2019, Atmospheric Pollution Research, https://doi.org/10.1016/j.apr.2019.02.010

Paoletti, E., De Marco, A., Beddows, D.C.S., Harrison, R.M., Manning, W.J.: Ozone levels in European and USA cities are increasing more than at rural sites, while peak values are decreasing, Environ. Pollut., 192, 295–299, https://doi.org/10.1016/j.envpol.2014.04.040, 2014.

Shanshan Zheng, Xiaofeng Xu, Yunjiang Zhang, Lingrui Wang, Yifan Yang, Shiguang Jin, Xiaoxiao Yang. Characteristics and sources of VOCs in urban and suburban environments in Shanghai, China, during the 2016 G20 summit. Atmospheric Pollution Research 10 (2019) 1766?1779

Shi, C., Wang, S., Liu, R., Zhou, R., Li, D., Wang, W., Li, Z., Cheng, T., Zhou, B.: A study of aerosol optical properties during ozone pollution episodes in 2013 over Shanghai, China, Atmos. Res., 153, 235–249, https://doi.org/10.1016/j.atmosres.2014.09.002, 2015.

Shu, L., Xie, M., Wang, T., Chen, P., Han, Y., Li, S., Zhuang, B., Li, M., Gao, D.: Integrated studies of a regional ozone pollution synthetically affected by subtropical high and typhoon system in the Yangtze River Delta region, China, Atmos. Chem. Phys. Discuss., 0, 1–32, https://doi.org/10.5194/acp-2016-581, 2016.

Sillman, S.: The relation between ozone, NO(x) and hydrocarbons in urban and polluted rural environments, Atmos. Environ., 33(12), 1821–1845, https://doi.org/10.1016/S1352-2310(98)00345-8, 1999.

Stauffer, D.R., Seaman, N.L., Binkowski, F.S.: Use of Four-Dimensional Data Assimilation in a Limited-Area Mesoscale Model Part II: Effects of Data Assimilation within the Planetary Boundary Layer, Mon. Weather Rev., https://doi.org/10.1175/1520-0493(1991)119<0734:UOFDDA>2.0.CO;2, 1991.

Su, W., Liu, C., Hu, Q., Fan, G., Xie, Z., Huang, X., Zhang, T., Chen, Z., Dong, Y., Ji, X., Liu, H., Wang, Z., Liu, J.: Characterization of ozone in the lower troposphere during the 2016 G20 conference in Hangzhou, Sci. Rep., 7, 17368, https://doi.org/10.1038/s41598-017-17646-x, 2017.

Tang, G., Li, X., Wang, Y., Xin, J., Ren, X.: Surface ozone trend details and interpretations in Beijing, 2001 – 2006, Atmos. Chem. Phys., 8813–8823, https://doi.org/10.5194/acpd-9-8159-2009, 2009.

Tang, G., Wang, Y., Li, X., Ji, D., Hsu, S., Gao, X.: Spatial-temporal variations in surface ozone in Northern China as observed during 2009-2010 and possible implications for future air quality control strategies, Atmos. Chem. Phys., 12, 2757–2776, https://doi.org/10.5194/acp-12-2757-2012, 2012.

Tang, G., Zhu, X., Xin, J., Hu, B., Song, T., Sun, Y., Wang, L., Cheng, M., Li, X., Wang, Y., Zhang, J., Chao, N., Kong, L., Li, X.: Modelling study of boundary-layer ozone over northern China - Part I: Ozone budget in summer, Atmos. Res., 187, 128–137, https://doi.org/10.1016/j.atmosres.2016.10.017, 2017a.

609 Teixeira, E., Fischer, G., van Velthuizen, H., van Dingenen, R., Dentener, F., Mills, G., Walter, C., Ewert, F.:
610 Limited potential of crop management for mitigating surface ozone impacts on global food supply, Atmos.
611 Environ., 45, 2569–2576, https://doi.org/10.1016/j.atmosenv.2011.02.002, 2011.
612 Tie, X., Geng, F., Guenther, A., Cao, J., Greenberg, J., Zhang, R., Apel, E., Li, G., Weinheimer, A., Chen, J., Cai,
613 C.: Megacity impacts on regional ozone formation: Observations and WRF-Chem modeling for the
614 MIRAGE-Shanghai field campaign, Atmos. Chem. Phys., 13, 5655–5669, https://doi.org/10.5194/acp-13-
615 5655-2013, 2013.
616 USEPA: Guidance on the Use of Models and Other Analyses for Demonstrating Attainment of Air Quality Goals
617 for Ozone, PM2.5 and Regional Haze, EPA-454/B-07e002. USEPA, 2007
618 von Schneidemesser, E., Coates, J., Denier van der Gon, H.A.C., Visschedijk, A.J.H., Butler, T.M.: Variation of
619 the NMVOC speciation in the solvent sector and the sensitivity of modelled tropospheric ozone, Atmos.
620 Environ., 135, 59–72, https://doi.org/10.1016/j.atmosenv.2016.03.057, 2016.
621 Wang, S., Xing, J., Chatani, S., Hao, J., Klimont, Z., Cofala, J., Amann, M.: Verification of anthropogenic
622 emissions of China by satellite and ground observations, Atmos. Environ., 45, 6347–6358,
623 https://doi.org/10.1016/j.atmosenv.2011.08.054, 2011.
624 Wang, T.J., Lam, K.S., Xie, M., Wang, X.M., Carmichael, G., Li, Y.S.: Integrated studies of a photochemical smog
625 episode in Hong Kong and regional transport in the Pearl River Delta of China, Tellus, Ser. B Chem. Phys.
626 Meteorol., 58, 31–40, https://doi.org/10.1111/j.1600-0889.2005.00172.x, 2006.
627 Wang, T., Xue, L., Brimblecombe, P., Lam, Y. F., Li, L. and Zhang, L.: Ozone pollution in China: A review of
628 concentrations, meteorological influences, chemical precursors, and effects, Sci. Total Environ., 575, 1582–
629 1596, https://doi.org/10.1016/j.scitotenv.2016.10.081, 2017.
630 Wang, Y., Hu, B., Tang, G., Ji, D., Zhang, H., Bai, J., Wang, X., Wang, Y.: Characteristics of ozone and its
631 precursors in Northern China: A comparative study of three sites, Atmos. Res., 132–133, 450–459,
632 https://doi.org/10.1016/j.atmosres.2013.04.005, 2013.
633 Wang, Y.H., Hu, B., Ji, D.S., Liu, Z.R., Tang, G.Q., Xin, J.Y., Zhang, H.X., Song, T., Wang, L.L., Gao, W.K.,
634 Wang, X.K., Wang, Y.S.: Ozone weekend effects in the Beijing-Tianjin-Hebei metropolitan area, China,
635 Atmos. Chem. Phys., 14, 2419–2429, https://doi.org/10.5194/acp-14-2419-2014, 2014.
636 Wu, K., Yang, X., Chen, D., Gu, S., Lu, Y., Jiang, Q., Wang, K., Ou, Y., Qian, Y., Shao, P. and Lu, S. (2020).
637 Estimation of biogenic VOC emissions and their corresponding impact on ozone and secondary organic
638 aerosol formation in China. Atmos. Res. 231: 104656.

639 Wu, L., Shen, J.D., Feng, Y.C., Bi, X.H., Jiao, L. and Liu, S.X. (2014). Source apportionment of particulate
640 matters in different size bins during hazy and non-hazy episodes in Hangzhou City. Res. Environ. Sci. 27:
641 373–381.
642 Xie, M., Zhu, K., Wang, T., Yang, H., Zhuang, B., Li, S., Li, M., Zhu, X., Ouyang, Y.: Application of
643 photochemical indicators to evaluate ozone nonlinear chemistry and pollution control countermeasure in
644 China, Atmos. Environ., 99, 466–473, https://doi.org/10.1016/j.atmosenv.2014.10.013, 2014.
645 Xue, L.K., Wang, T., Gao, J., Ding, A.J., Zhou, X.H., Blake, D.R., Wang, X.F., Saunders, S.M., Fan, S.J., Zuo,
646 H.C., Zhang, Q.Z., Wang, W.X.: Ground-level ozone in four Chinese cities: Precursors, regional transport
647 and heterogeneous processes, Atmos. Chem. Phys., 14, 13175–13188, https://doi.org/10.5194/acp-14-13175-
648 2014, 2014.
649 Yan, R.S., Li, L., An, J.Y., Lu, Q., Wang, S., Zhu, Y., Jang, C.J. and Fu, J.S. (2016). Establishment and application
650 of nonlinear response surface model of ozone in the Yangtze river delta region during summertime. Acta Sci.
651 Circumstant. 36: 1383–1392.
652 Zhang, B.N., Kim Oanh, N.T.: Photochemical smog pollution in the Bangkok Metropolitan Region of Thailand in
653 relation to O3 precursor concentrations and meteorological conditions, Atmos. Environ., 36, 4211–4222,
654 https://doi.org/10.1016/S1352-2310(02)00348-5, 2002.
655 Zhang, G., Xu, H., Qi, B., Du, R., Gui, K., Wang, H., Jiang, W., Liang, L. and Xu, W. (2018). Characterization of
656 atmospheric trace gases and particulate matter in Hangzhou, China. Atmos. Chem. Phys. 18: 1705–1728.
657 Zhang, H., Chen, G., Hu, J., Chen, S.H., Wiedinmyer, C., Kleeman, M., Ying, Q.: Evaluation of a seven-year air
658 quality simulation using the Weather Research and Forecasting (WRF)/Community Multiscale Air Quality
659 (CMAQ) models in the eastern United States, Sci. Total Environ., 473–474, 275–285,
660 https://doi.org/10.1016/j.scitotenv.2013.11.121, 2014.
661 Zhi-zhen Ni, Kun Luo, Jun-xi Zhang, Rui Feng, He-xin Zheng, Hao-ran Zhu, Jing-fan Wang, Jian-ren Fan, Xiang
662 Gao, Ke-fa Cen. Assessment of winter air pollution episodes using long-range transport modeling in
663 Hangzhou, China, during World Internet Conference, 2015. Environmental Pollution 236 (2018) 550-561